LRP 567/97 January 1997

THE KINX IDEAL MHD STABILITY CODE FOR AXISYMMETRIC PLASMAS WITH SEPARATRIX

L. Degtyarev, A. Martynov, S. Medvedev, F. Troyon, L. Villard, R. Gruber

Submitted for publication to
Computer Physics Communications

The KINX ideal MHD stability code for axisymmetric plasmas with separatrix

L.Degtyarev, A.Martynov, S.Medvedev

Keldysh Institute of Applied Mathematics, Russian Academy of Sciences, Moscow

F.Troyon, L.Villard [1]

Centre de Recherches en Physique des Plasmas, Association Euratom – Confédération Suisse, Ecole Polytechnique Fédérale de Lausanne

R.Gruber

Service Informatique Central, Ecole Polytechnique Fédérale de Lausanne

The paper presents the KINX code for computing linear ideal MHD growth rates and eigenvectors of axisymmetric plasmas surrounded by a vacuum layer and a conducting wall. Plasma equilibrium magnetic surfaces are assumed to be nested either in the whole plasma domain (separatrix at the plasma boundary is possible) or in the domains separated by an internal separatrix (doublet and divertor configurations). The computational domain is decomposed into subdomains with nested flux surfaces. In each subdomain finite hybrid elements are used on an equilibrium grid adapted to magnetic surfaces. Numerical destabilization is eliminated; this results in better convergence properties and makes possible efficient stability index calculation (δW–code). An inverse vector iteration method and a vectorizable matrix solver are applied to the matrix eigenvalue problem. Stability studies of external kink modes for doublet and single null configurations are given as application examples of the KINX code. Another version of the code, KINX-W, computing resistive wall $n = 0$ mode growth rates is also presented for single null, doublet and divertor plasma configurations.

PACS: 52.65.Kj, 52.35.Py, 52.30.Bt, 52.55.Fa.
Keywords: Magnetohydrodynamics, macroinstabilities, tokamak, separatrix, finite elements, spectrum.

[1] Corresponding author: L. Villard, CRPP-PPB, EPFL, 1015 Lausanne, Switzerland, tel: +41 21 693 4564, fax: +41 21 693 5176, e-mail: villard@crpp.epfl.ch

1 Introduction

Equilibrium and stability computations are an important part of theoretical investigations of tokamak plasma physics and interpretation of experimental data. Several MHD stability codes have been developed during the last twenty years to satisfy these needs [1–6]. However the self-consistent modeling of plasmas with separatrix inherent to divertor configurations and investigations of doublets with internal separatrix are beyond the scope of most of the codes. The reason for that is the use of the flux coordinates in the problem formulation. Indeed, the ideal MHD equation anisotropy – different derivative orders of tangential displacement within and across magnetic surfaces – forces the use of the computational grids aligned with magnetic surfaces. The coordinate transformation to the flux coordinates connected with magnetic surfaces is not regular in the configurations with a separatrix. In the codes with Fourier decomposition in the poloidal angle, this results in a large number of harmonics needed for the solution representation. The finite element codes are more suitable to treat the associated singularities. The domain decomposition into several subdomains with nested flux surfaces makes possible the computations of the divertor and doublet configurations.

The use of hybrid finite elements gives a family of difference schemes which do not pollute the MHD spectrum. However, the numerical destabilization results in a convergence from below to the spectrum lower boundary and therefore difficulties in marginal stability determination. The elimination of the destabilization makes possible an efficient calculation of the stability index using the reduced ideal MHD stability problem (δW-code) with different spectrum structure.

The KINX code presented in the paper has proven to be a useful tool of stability analysis for different types of tokamak plasma configurations. Examples of the code applications are given in the Section 4.

2 Formulation of the problem

2.1 Potential energy representation

Linearized ideal MHD eigenvalue equations for a plasma displacement $\vec{\xi}e^{i\omega t}$ from an equilibrium can be written in the weak form [7]:

$$W(\vec{\xi},\tilde{\vec{\xi}}) - \omega^2 K(\vec{\xi},\tilde{\vec{\xi}}) = 0, \qquad (1)$$

where $\tilde{\vec{\xi}}$ is an arbitrary trial vector. The quadratic functionals $W(\vec{\xi},\vec{\xi})$ and $\omega^2 K(\vec{\xi},\vec{\xi})$ correspond to potential and kinetic energies of the plasma displacement. A negative eigenvalue ω^2 gives an unstable solution growing in time.

The following projections of the vector $\vec{\xi}$ are used

$$\vec{\xi} = \xi^{\psi}\frac{\vec{D}\times\vec{B}}{|\vec{B}|^2} + \xi^{D}\frac{\vec{B}\times\nabla\psi}{|\vec{B}|^2} + \xi^{B}\frac{\vec{B}}{|\vec{B}|^2}, \tag{2}$$

where $\vec{B}$ is the equilibrium magnetic field

$$\vec{B} = \nabla\psi\times\nabla\phi + F(\psi)\nabla\phi = \nabla\psi\times\vec{D}, \tag{3}$$

$\xi^{\psi} = \vec{\xi}\cdot\nabla\psi$, ϕ is the toroidal angle. The functionals W and K can be represented as follows [8]:

$$\begin{aligned} W &= W_p + W_v, \qquad (4)\\ W_p &= \frac{1}{2}\int_{V_p}\{|\nabla\times(\vec{\xi}\times\vec{B})|^2 + 2\xi^{\psi}(\vec{j}\cdot\nabla\xi^{D}) + \frac{dp}{d\psi}\nabla\cdot\left(\frac{\partial\vec{r}}{\partial\psi}|\xi^{\psi}|^2\right)\\ &\quad + \frac{\nabla\psi\times\vec{j}}{|\nabla\psi|^2}\cdot\nabla\times\vec{D}|\xi^{\psi}|^2 + \Gamma p|\nabla\cdot\vec{\xi}|^2\}\,dV,\\ K &= \frac{1}{2}\int_{V_p}\rho_p\{|\xi^{\psi}|^2\frac{|\vec{D}|^2}{|\vec{B}|^2} - 2\xi^{\psi}\xi^{D}\frac{\vec{D}\cdot\nabla\psi}{|\vec{B}|^2} + |\xi^{D}|^2\frac{|\nabla\psi|^2}{|\vec{B}|^2} + |\xi^{B}|^2\frac{1}{|\vec{B}|^2}\}\,dV, \end{aligned}$$

where $\vec{j}$ is the current density $\vec{j} = \nabla\times\vec{B}$, Γ is the adiabatic index, p is the plasma pressure, ρ_p is the plasma density, V_p is the plasma volume, W_v is the vacuum part of the potential energy.

The flux coordinate system (ψ,θ,ϕ) with Jacobian $\sqrt{g} = (\nabla\psi\times\nabla\theta\cdot\nabla\phi)^{-1}$ is used where $\psi = const$ mark magnetic surfaces, θ is a poloidal variable and ϕ is the toroidal angle. In the flux coordinate system the first term in the expression (4) for W can be rewritten as follows:

$$\begin{aligned} &\int|\nabla\times(\vec{\xi}\times\vec{B})|^2\,dV = \int\frac{g_{kl}}{\sqrt{g}}Q^kQ^l\,d\psi d\theta d\phi, \qquad (5)\\ &Q^1 = \frac{\partial\xi^{\psi}}{\partial\theta} + \nu\frac{\partial\xi^{\psi}}{\partial\phi}, \quad Q^2 = \frac{\partial\xi^{\psi}}{\partial\psi} + \frac{\partial\xi^{D}}{\partial\phi}, \quad Q^3 = \frac{\partial(\xi^{\psi}\nu)}{\partial\psi} - \frac{\partial\xi^{D}}{\partial\theta}, \end{aligned}$$

where g_{kl} and $\sqrt{g}$ are metric coefficients and Jacobian of the coordinate system, $\nu = -\sqrt{g}F/r^2$, (r,z,ϕ) are cylindrical coordinates. There are no ψ–derivatives

of the components ξ^D and ξ^B entering the functional W. This fact leads to a noncompactness of the operator corresponding to the equation (1) and gives a spectrum containing continuous parts and accumulation points [9].

For an axisymmetric equilibrium Fourier modes $\vec{\xi}_n e^{in\phi}$ with different toroidal wave numbers n are decoupled and the equation (1) becomes a two–dimensional eigenvalue problem for each $\vec{\xi}_n$.

2.2 Vacuum

The vacuum part of the potential energy functional (4) is

$$W_v = \frac{1}{2} \int_{V_v} |\nabla \times \vec{A}|^2 \tag{6}$$

where $\vec{A}$ is a vector potential of the vacuum magnetic field perturbation $\delta \vec{B}_v = \nabla \times \vec{A}$. At the ideally conducting wall

$$\vec{n} \times \vec{A} = 0. \tag{7}$$

The boundary condition at the plasma – vacuum interface is given by the to tangential electric field continuity across the interface:

$$\vec{n} \times \vec{A} = \vec{n} \times (\vec{\xi} \times \vec{B}) \tag{8}$$

Then the total pressure continuity is a natural boundary condition for the variational formulation (1).

The Euler equation of the functional (6)

$$\nabla \times \nabla \times \vec{A} = 0 \tag{9}$$

together with the boundary conditions (7), (8) specifies the vacuum problem.

2.3 δW-code

To find only the stability index — the sign of the lowest eigenvalue — it is sufficient to use some other norm instead of the kinetic energy to minimize

the potential energy (δW-code). It can be chosen as a positive functional of only one displacement component ξ^ψ:

$$K_1 = \frac{1}{2}\int \rho_p \{|\xi^\psi|^2 \frac{1}{|\nabla\psi|^2}\}\, dV. \tag{10}$$

This choice of the norm changes the spectrum structure, shifting the continuous spectrum in such a way that unstable eigenvalue branches can be traced into the stable part of the spectrum [10]. It is important for stability limits computations.

The specific features of the spectrum of the reduced ideal MHD eigenproblem are generated by the singularity in the potential energy functional $W_1 = \min_{\xi D} W$ after minimization against the tangential components of the displacement: the derivative $\partial\xi^\psi/\partial\psi$ enters the reduced functional under the operator $\vec{B}\nabla$. The kernel of the operator $\vec{B}\nabla$ includes so called resonant harmonics $\vec{\xi}_{mn}e^{i(m\theta+n\phi)}$ with poloidal and toroidal wave numbers m, n satisfying $m + nq(\psi_s) = 0$ at the resonant surfaces $\psi = \psi_s$ in plasma, where $q(\psi) = 1/2\pi \int \nu d\theta$ is the safety factor. To study the behavior of the eigenfuctions at a resonant surface one can consider the displacements localized near the surface. Then the Rayleigh quotient of the reduced problem takes the form [11]

$$W_1/K_1 = \tag{11}$$
$$\int_1^{-1} dy \left(\frac{1}{< |\vec{B}|^2/|\nabla\psi|^2 >} \left| < S > y\frac{d\xi_0}{dy} - < T > \xi_0 \right|^2 - < k > |\xi_0|^2 \right)$$
$$/ \int_1^{-1} dy \left(< \rho_p/|\nabla\psi|^2 > |\xi_0|^2 \right)$$

where $y = (\psi - \psi_s)/\epsilon$, $\epsilon \to 0$, $\xi_0(y)$ is the lowest order in ϵ of the ξ^ψ resonant harmonic,

$$T = (\vec{j}\cdot\vec{B})/|\nabla\psi|^2 - S, \quad S = \vec{B}\times\nabla\psi/|\nabla\psi|^2 \cdot \nabla \times (\vec{B}\times\nabla\psi/|\nabla\psi|^2),$$

$$k = 2\frac{\vec{j}\times\nabla\psi}{|\nabla\psi|^2}\cdot(\vec{B}\nabla)\nabla\psi,$$

and the averaging is defined as

$$< f >= \frac{1}{4\pi^2}\int\int f\sqrt{g}d\theta d\phi.$$

The corresponding characteristic equation for $\xi_0 = y^\alpha$ implies that

$$\alpha = -\frac{1}{2} \pm (D_M - G\omega^2)^{1/2}, \tag{12}$$

$$D_M = \frac{1}{4} + \left(< S >< T > + < T >^2 - < k >< |\vec{B}|^2/|\nabla\psi|^2 > \right) / < S >^2 ,$$

$$G = < \rho_p/|\nabla\psi|^2 >< |\vec{B}|^2/|\nabla\psi|^2 > / < S >^2,$$

where D_M is the expression for the Mercier criterion, $D_M < 0$ corresponds to instability.

From (12) it follows that negative values of $(D_M - G\omega^2)$ correspond to nonintegrable solutions giving rise to the continuous spectrum. The lower boundary of the continuum is $\omega^2 = \omega_M = D_M/G$. So if the configuration is Mercier stable, $D_M > 0$, then the boundary of the continuum shifts into the $\omega^2 > 0$ region. This is in contrast with the full normalization problem where the Alfvén continuous spectrum boundary $\omega^2 \sim \min_\psi (m + nq(\psi))^2 = 0$ if a resonant surface exists in the plasma.

Near the magnetic axis the asymptotic behavior of eigenfunctions can be described in the frame of a cylindrical model. For any harmonic numbers m, n the Euler equation of the reduced problem takes the following form

$$-y(y\xi')' + m^2(1 - \omega^2/\omega_A^2)\xi = 0, \tag{13}$$

where the derivatives are in y — minor radius coordinate, $\xi = \xi^\psi$, $\omega_A^2 = (B_\theta/y)^2(m+nq)^2/\rho_p$ is the Alfvén frequency at the axis. This gives the asymptotic dependence

$$\alpha = |m|(1 - \omega^2/{\omega_A}^2)^{1/2}, \quad \xi^\psi \sim y^\alpha. \tag{14}$$

For a finite plasma density ρ_p on axis the asymptotic behavior of the eigenfunctions of the reduced problem differs from that of the full problem where $\xi^\psi \sim y^{|m|}$. From (14) also follows that in the reduced problem there exists one more continuum spectrum branch $\omega^2 \geq {\omega_A}^2$. Depending on the value of q on axis the value of ${\omega_A}^2$ can be close to zero, again making the marginal stability computations more difficult. To avoid it the density function $\rho_p(\psi)$ can be chosen so that $\rho_p(\psi) \sim \bar{\psi}$ near axis where $\bar{\psi}$ is the normalized poloidal flux vanishing near axis. Then ${\omega_A}^2 \to \infty$ and the additional continuum disappears while eigenfunctions restore the asymptotic behavior $\xi^\psi \sim y^{|m|}$ at the axis. The choice $\rho_p \sim |\nabla\psi|^2$ in the PEST-2 code [10] satisfies the above requirements.

2.4 *Resistive wall in vacuum*

To include the effect of the resistive wall into the model it is sufficient to rewrite the functional W_v in the following form:

$$W_v = \frac{1}{2}\int\limits_{S_p} \vec{B}\cdot\delta\vec{B}_v(\vec{n}\cdot\tilde{\vec{\xi}})\,dS, \tag{15}$$

where S_p is the plasma–vacuum interface surface, $\vec{n}$ is an external normal to S_p. The problem (1) can be reduced to an eigenvalue problem (nonlinear in general) for $\vec{\xi}$ as soon as $\delta\vec{B}_v$ is known in terms of ξ^ψ on S_p.

For axisymmetric $n = 0$ modes the following representations for $\delta\vec{B}_v$ in the vacuum can be used [12]:

$$\delta\vec{B}_v = \nabla\chi\times\nabla\phi + a_t\nabla\phi, \tag{16}$$

with the boundary condition at the plasma surface S_p

$$\chi = -\xi^\psi.$$

From $\nabla\times\delta\vec{B}_v = 0$ in the vacuum region follows the equation for χ:

$$\nabla\cdot\left(\frac{\nabla\chi}{r^2}\right) = 0, \quad |\chi|\to 0, |\vec{r}|\to\infty. \tag{17}$$

The equation (17) is supplemented with the boundary condition at the resistive wall using the thin–wall approximation:

$$[\![\vec{n}\cdot\nabla\chi]\!] = \frac{i\omega}{\eta}\chi, \tag{18}$$

where $[\![\cdot]\!]$ is the jump across the surface of the wall, η is the ratio of the wall toroidal resistivity to the wall thickness. The relation between the value of $\vec{n}\cdot\nabla\chi$ needed for the evaluation of (15) and χ at the plasma boundary can be found using a Green's function technique. The value of a_t can be expressed directly in terms of ξ^ψ at the plasma boundary:

$$a_t = -i\omega\left(\int\limits_0^{2\pi}\xi^\psi\nu\,d\theta\right)\Big/\left(i\omega\int\limits_{S_{tor}}\frac{drdz}{r} + \int\limits_{C_w}\eta_{pol}\frac{dl}{r}\right), \tag{19}$$

where $\nu = -F\sqrt{g}/r^2$, S_{tor} is the toroidal cross section between the plasma and the wall, C_w is the wall contour in the plane $\phi = const$ and η_{pol} is the ratio of the wall poloidal resistivity and the wall thickness.

For modes with $n \neq 0$ the perturbed magnetic field in the vacuum is represented by a scalar potential Φ

$$\delta\vec{B}_v = \nabla\Phi, \quad \nabla^2\Phi = 0,$$

with the boundary condition

$$\frac{d\Phi}{d\vec{n}} = \frac{\vec{n}\cdot\nabla\psi}{|\nabla\psi|}\frac{1}{rdl/d\theta}\left(\frac{\partial\xi^\psi}{\partial\theta} + in\nu\xi^\psi\right),$$

at the plasma vacuum boundary contour l. At the ideally conducting wall the boundary condition is

$$\frac{d\Phi}{d\vec{n}} = 0.$$

The jump of the potential $\Delta\Phi$ across the resistive wall is related to the derivative at the wall through the boundary condition directly following from Faraday's and Ohm's laws for thin wall approximation [13]

$$i\omega\frac{d\Phi}{d\vec{n}} = -n^2\eta\frac{\Delta\Phi}{r^2} + \frac{1}{r\sqrt{r_\theta^2 + z_\theta^2}}\frac{\partial}{\partial\theta}\left(\eta\frac{r}{\sqrt{r_\theta^2 + z_\theta^2}}\frac{\partial\Delta\Phi}{\partial\theta}\right)$$

where $r_\theta = \partial r/\partial\theta$, $z_\theta = \partial z/\partial\theta$. Using a Green's function technique the values of Φ at the plasma boundary can be expressed in terms of $d\Phi/d\vec{n}$ at the plasma–vacuum boundary.

3 Numerical method

3.1 Approximation

The flux coordinates and hybrid finite elements [14] are used to ensure the spectral convergence [9]. The main requirement here is to choose for the tangential components ξ^D, ξ^B basis functions one order lower in the flux variable ψ than for the normal component ξ^ψ. The additional property of the hybrid

finite element method is the use of different basis functions not only for different displacement components but also for different derivatives of the same unknown, thus making the approximation of all terms in the potential energy functional constant in a mesh cell. This choice of discretization helps to decouple the different branches of the MHD spectrum.

Each subdomain with nested flux surfaces in doublet or divertor equilibrium configurations can be treated in the same way as a single axis plasma. The calculations of matrix elements are performed separately for each subdomain. The connectivity conditions between the subdomains involve only the values of the component ξ^ψ at the separatrix. The connectivity condition at the x-point of the separatrix is replaced by the regularity condition $\xi^\psi = 0$ (the same as at the magnetic axes). The remaining connectivity conditions are applied in the matrix solver.

The minimization of the vacuum energy functional can be performed using the Green's function technique (boundary finite elements) [1,2]. This method can be applied for a wide range of plasma and external conductor topologies. At the same time the resistive wall effects can be included in the formulation in a straightforward manner [12,13]. Another approach to the vacuum treatment is the use of a special gauge of the perturbed vacuum field vector potential $\vec{A} = \vec{\xi}_v \times \vec{B}_{ps}$ — with the "pseudodisplacement" $\vec{\xi}_v$ [15]. The vector field $\vec{B}_{ps}$ should not coincide with the equilibrium vacuum magnetic field but ensure the gauge correctness. The representation of $\vec{B}_{ps}$ in a form similar to (3) and the use of the same displacement projections (2) lead to an approximation similar to the plasma functional. This approach provides the same convergence order as for plasma approximation and makes the convergence studies easier. Both methods are implemented in different versions of the KINX code.

3.2 Grid adapted to magnetic surfaces

The non-polluting spectrum approximation requires a special choice of the basis functions in the flux coordinates. It requires a mapping of magnetic surfaces which are level lines of the poloidal flux function ψ. The poloidal θ variable can be fixed by prescribing the Jacobian to fulfil the straight magnetic field line condition for example [2]. Such a choice is however singular at the x-point of the separatrix and is not suitable for our purpose. Another choice is to define the Jacobian from the grid cell geometry and make the approximation of the stability functionals (4) invariant against the choice of θ variable. The approximation of the metric coefficients in the KINX code fulfils this requirement.

The accurate mapping of magnetic surfaces is a complicated and time consum-

ing task. One of the efficient ways to do it simultaneously with the equilibrium equation solution is to adapt the grid to magnetic surfaces [16,17]. The code CAXE [18] has been developed to compute the MHD equilibrium on a grid adapted to magnetic surfaces for single axis and doublet configurations. The domain decomposition into four subdomains with nested flux surfaces is used for doublet equilibria computations. The interface from the CAXE code to the KINX code includes

- quasi–polar quadrangular grid adapted to nested magnetic surfaces in each subdomain. The grid is described by a single function ρ_{ij}:

$$\begin{aligned} r_{ij} &= r_{mj} + \rho_{ij}(r_{kj} - r_{mj}), \\ z_{ij} &= z_{mj} + \rho_{ij}(z_{kj} - z_{mj}), \end{aligned} \tag{20}$$

  where r_{mj}, z_{mj} and r_{kj}, z_{kj} are the coordinates of the inner and the outer domain boundaries, $0 \leq \rho \leq 1$. Magnetic surfaces are given by $i = const.$ The representations implies $j = const$ to be straight lines.
- flux grid and flux functions in each domain. The values $\{s_i\}$ of the function $s = (\psi - \psi_{in})/(\psi_{out} - \psi_{in}), \quad 0 \leq s \leq 1$ are used to mark the magnetic surfaces. The flux functions $p' = dp/d\psi$ and FF' are given for $s = s_i$.

3.3 Elimination of numerical destabilization and spectral shift

Some further modifications of the approximation are used to improve the convergence in the KINX code: the numerical destabilization correction [19] and the spectral shift elimination [14].

The spectral convergence is ensured by the hybrid finite elements. However, the marginal stability $\omega^2 = 0$ belongs to the MHD spectrum when rational magnetic surfaces are present in plasma. The numerical destabilization means convergence from the unstable side $\omega^2 < 0$ to the stability boundary $\omega^2 = 0$. Without the correction of the destabilization the computations of the stability index — the sign of the lowest eigenvalue — require convergence studies. In [19] it was shown that the numerical destabilization was connected with a loss of spectral convergence for the reduced problem with the norm (10) because of the vanishing coefficient at the highest order derivative in equation (11). The numerical destabilization correction makes possible a direct transformation of the code into δW–code ensuring spectral convergence also for the reduced problem. The correction term to the hybrid finite element approximation is derived from the analysis of localized modes described by (11). The correction lower estimate is given by the following additional term to the potential energy

functional approximation

$$-\frac{1}{2}\int \frac{(h^{\psi})^2}{<|\vec{B}|^2/|\nabla\psi|^2>}\left(\frac{<S><T>}{4}+\frac{<S>^2}{8}\right)\left(\frac{\partial\xi^{\psi}}{\partial\psi}\right)^2 d\psi \qquad (21)$$

where h^{ψ} is the mesh step in ψ.

It was shown in [14] that the exact equality $(\vec{B}\nabla\xi)=0$ at rational surfaces for resonant harmonic can be fulfilled by a small correction of the toroidal wave number n value. It was applied to eliminate the spectral shift in the ERATO code where hybrid finite elements and straight magnetic field line coordinates were used. The idea can be directly extended to any flux coordinate system.

In the KINX code the use of hybrid finite elements in θ-direction leads to the following approximation of the operator $(\vec{B}\nabla)$:

$$(\vec{B}\nabla\xi)\sim\frac{\xi_{j+1}-\xi_j}{h^{\theta}_{j+1/2}}+in\nu_{j+1/2}\frac{\xi_{j+1}+\xi_j}{2}, \qquad (22)$$

where h^{θ} is the mesh step in θ. To ensure its vanishing for resonant harmonic at rational surfaces the toroidal wave number n should be replaced by

$$n_{j+1/2}=\frac{2}{\nu_{j+1/2}h^{\theta}_{j+1/2}}\tan(n\nu_{j+1/2}h^{\theta}_{j+1/2}/2).$$

Taking into account the relation

$$\nu_{j+1/2}h^{\theta}_{j+1/2}=qh^{\bar{\theta}}_{j+1/2}$$

with $\bar{\theta}$ corresponding to straight field line coordinates, the expression (22) for the harmonic $e^{il\bar{\theta}_j}$ is

$$\frac{2}{h^{\bar{\theta}}_{j+1/2}}\frac{sin[(l+nq)h^{\bar{\theta}}_{j+1/2}/2]}{cos(lh^{\bar{\theta}}_{j+1/2}/2)cos(nqh^{\bar{\theta}}_{j+1/2}/2)}e^{il\bar{\theta}_j} \qquad (23)$$

vanishing for $l+nq=0$.

3.4 Eigenvalue solver

The matrix solver is based on the package PAMERA [20]. The matrix of the problem consists of banded blocks. Nonoverlapping blocks can be efficiently

inverted beforehand [21]. The resulting matrix structure is block 3-diagonal. Then for each subdomain the block elimination is performed separately up to the connectivity unknowns. The connectivity assembling consists of the overlapping of the resulting full blocks with the proper numbering. The solver performance is high if full matrix operations are performed with optimized routines on a vector computer. The inverse iteration converges to the eigenvalue which is the nearest to an initial guess. Due to matrix symmetry an additional information on the number of the eigenvalues less than the initial guess is obtained during the matrix inversion.

A typical stability computation for a single axis plasma with grid dimensions $N_\psi = N_\theta = 128$ requires about 800Mb of memory and takes 25s of the NEC SX4 single CPU at the speed of 900Mflops. A doublet computation with $N_\psi = N_\theta = 96$ in each of the two subdomains inside the separatrix and $N_\psi = 48, N_\theta = 192$ in the subdomain outside the separatrix takes 35s with the same resources and performance.

4 Examples of stability computations

Optimization of tokamak fusion reactors requires the value of $\beta = 2\mu_0 < p > /B_c^2$ to be maximized. Here $< p >$ is the pressure averaged over the plasma volume and B_c is the vacuum toroidal magnetic field taken at the plasma center. The stability of external kink modes sets the limit to the plasma pressure. The limiting β-values were found to be proportional to the normalized plasma current $I_N = I[MA]/(a[m]B_c[T])$ [22], giving for conventional tokamaks the scaling $\beta = gI_N$, where I is the plasma current and a is the plasma minor radius. The computations with the KINX code make possible further investigations of the tokamak MHD stability limits.

4.1 Kink modes in single null plasma with separatrix at the boundary

Stability computations of the plasma with a separatrix at the boundary are possible with the KINX code. An example of $n = 1$ external pressure driven kink mode calculation is given below. The plasma profiles (Fig.1) correspond to an ITER H-mode equilibrium [23]. The normalized value of $g = \beta/I_N = 6.4\%$ is above the external kink pressure limit.

The separatrix geometry was computed with the free boundary code for given ITER poloidal field coil currents. More detailed equilibrium computations were performed with a prescribed separatrix as a plasma boundary with the fixed boundary equilibrium code CAXE [18].

The eigenfunction structure is presented in Fig.2. Fig.3 show the convergence of the eigenvalues normalized by the Alfvén frequency at the plasma center ω_A^2 with equal numbers of radial and poloidal grid points $N_\psi = N_\theta = N$. Both the eigenvalues of the problem with kinetic energy normalization and the δW normalization (10) with $\rho_p = \bar{\psi}$ are given. The growth rate for the equilibrium with the separatrix at the boundary is lower than for the equilibrium with the plasma boundary truncated at the value of normalized poloidal flux $\bar{\psi} = 0.95$. The convergence rate is $1/N^2$ in both cases and the slopes of the convergence curves are close to each other.

The β limit studies in ITER [23] performed with the KINX code showed that the limiting values of g are higher in the configuration with the separatrix at the boundary than in one with the $\bar{\psi} = 0.95$ boundary by a factor of approximately 1.1. Moreover, no drops in the β values corresponding to the rational values of the safety factor q_s at the boundary and no peeling mode instability were found with the separatrix at the boundary.

4.2 Kink modes in doublets

The external kink β limit for doublet configurations with pressureless and currentless mantle outside the separatrix were found to be very close to the single axis plasma limits [24]. Finite equilibrium current and pressure gradient outside the separatrix give rise to instabilities with different properties.

One of the examples is the outer peeling mode driven by the finite current density at the plasma edge outside the separatrix [25]. The corresponding doublet equilibria were computed by the CAXE code with the fixed boundary fitted into the TCV vacuum chamber. The plasma profiles, with pressure gradient having a maximum at the separatrix and finite separatrix current density, were prescribed by

$$\begin{aligned} I^* &= 1 - (1 - I_s)\bar{\psi}^{in}, \quad p' = p_0\bar{\psi}^{in}, \quad \text{inside separatrix} \\ I^* &= I_s(1 - \bar{\psi}^{out}), \quad p' = p_0(1 - \bar{\psi}^{out}), \quad \text{outside separatrix} \end{aligned} \tag{24}$$

where I^* is the surface averaged toroidal current density, $0 < \bar{\psi}^{in,out} < 1$ are the normalized poloidal fluxes inside and outside the separatrix, respectively, I_s is the value of the current density at the separatrix, p_0 is the maximal value of the pressure gradient at the separatrix. The value of the safety factor at the magnetic axis is $q_0 = 1.05$.

Equilibria with finite current density at the boundary can be generated by removing the outer magnetic surfaces from the plasma boundary. The peeling mode structure for the value of the normalized left flux outside the separatrix

$\psi_s = 0.374$ is given in Fig.4 for a force-free equilibrium with $I_s = 0.1$. The conducting wall is assumed to be far from the plasma boundary. The corresponding eigenvalue $-\omega^2/\omega_A$ convergence is shown in Fig.5 for numbers of grid points inside the separatrix $N_\psi = N_\theta = N$ and outside the separatrix $N_\psi = N/4, N_\theta = 2N$.

The coupling between the regions inside and outside the separatrix is characteristic for the $n = 1$ pressure driven external kink mode at finite value of $g = 2.4\%$ (Fig.6 and Fig.7). Having finite current density and pressure gradient in the plasma outside separatrix reduces the limiting value of g from $g = 1.8\%$ (when the outside plasma is replaced by vacuum) to $g = 1.6\%$ despite the finite current density at the plasma boundary in the first case. The difference is bigger if the pressure profile outside the separatrix is steeper. Note that the values of g for the doublet plasma should be doubled to be compared with the corresponding single axis plasma values, because the plasma current in the doublet is about twice that in each of the domains inside the separatrix.

4.3 Resistive wall axisymmetric modes in doublet and divertor configurations

The axisymmetric mode growth rate in doublet configurations is close to that of the single axis plasma inside the separatrix and therefore much lower than that of a single axis plasma with the same overall elongation [24].

Fig.8 presents the mode structure of the two unstable modes for the force-free equilibrium (24) with $I_s = 0$. The resistive wall is taken to coincide with the TCV vacuum chamber having the cross section averaged resistance $4.4 \cdot 10^{-5}[Ohm]$. The growth rate convergence curves are given in Fig.9.

The most unstable mode has up-down symmetric and the second mode has antisymmetric normal displacement component. Stabilizing perturbed surface current at the plasma boundary is present only for up-down nonsymmetric single axis plasma and vanishes in the up-down symmetric case [26]. In doublets the surface current perturbation has a stabilizing influence on the most unstable mode due to its symmetric structure. The growth rate of the most unstable mode increases from $240[s^{-1}]$ up to $630[s^{-1}]$ when the outside plasma is replaced by vacuum while the growth rate of the second mode remains unchanged.

Divertor equilibrium configurations can also be treated by the KINX code. One of the important questions is a choice of the boundary conditions at the open equilibrium field lines. The vanishing displacement condition ensures the variational principle existence [26,25].

In Fig.10 the $n = 0$ mode structure for the divertor equilibrium with the

boundary and profiles corresponding to the above doublet equilibrium is presented. The convergence of the corresponding growth rate is shown in Fig.11.

Acknowledgement

This work was partly supported by the Swiss National Science Foundation.

References

[1] R.C. Grimm, J.M. Greene and J.L. Johnson, in: *Methods of Computational Physics* **16** (Academic Press, New York London, 1976) 253.

[2] R. Gruber, F. Troyon, D. Berger, L.C. Bernard, S. Rousset, R. Schreiber, W. Kerner, W. Schneider and K.V. Roberts, *Comput. Phys. Commun.* **21** (1981) 323.

[3] R. Gruber, F. Troyon, S. Rousset, W. Kerner and L.C. Bernard, *Comput. Phys. Commun.* **22** (1981) 383.

[4] L.C. Bernard, F.J. Helton and R.W. Moore, *Comput. Phys. Commun.* **24** (1981) 377.

[5] C.Z. Cheng and M.S. Chance, *J. Comput. Phys.* **71** (1987) 124.

[6] A. Bondeson, G. Vlad and H. Lütjens, *Phys. Fluids B* **4** (1992) 1889.

[7] I.B. Bernstein *et al. Proc.Roy. Soc.* **A244** (1958) 17.

[8] S.A. Galkin, V.V. Drozdov and A.A. Martynov, Variational approach to constructing approximate models for MHD equilibrium and stability, *Preprint of Keldysh Inst. Appl. Math.* N 152 (1991).

[9] J. Rappaz, *Numer. Math.* **28** (1977) 15.

[10] R.C. Grimm, R.L. Dewar and J. Manickam, *J. Comput. Phys.* **49** (1983) 94.

[11] J.M.Greene and J.L.Johnson, *Phys. Fluids* **5** (1962) 510.

[12] D.J. Ward, S.C. Jardin and C.Z.Cheng, *J. Comput.Phys.* **104** (1993) 221.

[13] D.J. Ward and A. Bondeson, *Phys. Plasmas* **2** (1995) 1570.

[14] R. Gruber, *J. Comput. Phys.* **26** (1978) 379.

[15] R. Gruber, S. Semenzato, F. Troyon, T. Tsunematsu, W. Kerner, P. Merkel and W. Schneider, *Comput. Phys. Commun.* **24** (1981) 363.

[16] L.M. Degtyarev and V.V. Drozdov, *Comput. Phys. Reports* **2** (1985) 341.

[17] S. Semenzato, R. Gruber and H.P. Zehrfeld, *Comput. Phys. Reports* **1** (1984) 389. R. Gruber, R. Iacono and F. Troyon, *J. Comput. Phys.* **73** (1987) 168.

[18] S.Yu. Medvedev, L. Villard, L.M. Degtyarev, A.A. Martynov, R. Gruber and F. Troyon, MHD equilibrium and stability of doublet configurations, *20th EPS Conf. on Controlled Fusion and Plasma Phys., Lisbon, Proc. Contrib. Papers* Vol. 17C, part IV (1993) 1279.

[19] L.M. Degtyarev and S.Yu. Medvedev, *Comput. Phys. Commun.* **43** (1986) 29.

[20] R. Gruber, W.A. Cooper, M. Beniston, M. Gengler and S. Merazzi, *Phys. Reports* **207** (1991) 167.

[21] D.S. Scott and R. Gruber, *Comput. Phys. Commun.* **23** (1981) 115.

[22] F. Troyon, R. Gruber, H. Saurenmann, S. Semenzato and S. Succi, *Plasma Phys. and Contr. Fusion* **26** (1984) 209.

[23] M. Rosenbluth, J. Hogan, D. Boucher *et al.*, ITER plasma modeling and MHD stability limits, *Proc. 5th Int. Conf. on Plasma Phys. and Controlled Nuclear Fusion Research, Sevilla, Spain, September-October 1994* , IAEA, Vienna (1995) Vol.2, 517.

[24] L.M. Degtyarev, A.A. Martynov, S.Yu. Medvedev, F.Troyon and L.Villard, MHD limits and axisymmetric stability of doublets, *21st EPS Conf. on Controlled Fusion and Plasma Phys., Montpellier, Proc. Contrib. Papers* vol.18B, Part II (1994) 556.

[25] L.M. Degtyarev, A.A. Martynov, S.Yu. Medvedev, F. Troyon and L.Villard, External kink mode stability of tokamaks with finite edge current density in plasma outside separatrix, *23rd EPS Conf. on Controlled Fusion and Plasma Phys., Kiev, Proc. Contrib. Papers* (1996) paper g006, to appear.

[26] L.M. Degtyarev, A.A. Martynov, S.Yu. Medvedev, F. Troyon and L.Villard, Influence of plasma near separatrix on ideal MHD stability in tokamaks, *22nd EPS Conf. on Controlled Fusion and Plasma Phys., Bournemouth, Proc. Contrib. Papers* vol.19C, Part I (1995) 217.

Figure captions

Fig.1. Profiles of the safety factor q (top), the parallel current density $< j \cdot B >$ (middle) and pressure profile p' (bottom) for an ITER H-mode equilibrium. The pressure gradient profile locally optimized against ballooning mode stability is shown by a dashed line.

Fig.2. External kink mode structure for the ITER H-mode equilibrium with the separatrix at the boundary. Normal displacement level lines (left) and displacement arrow plot (right).

Fig.3. Convergence of the external kink mode eigenvalues $-\omega^2/\omega_A^2$ for the ITER H-mode equilibrium. Kinetic energy (a,b) and δW (c,d) normalizations. Two curves at each plot correspond to the equilibrium with $\bar{\psi} = 0.95$ boundary (a,c) and the equilibrium with the separatrix at the boundary (b,d).

Fig.4. Peeling mode structure for the doublet equilibrium with finite current density at the boundary. Normal displacement level lines (left) and displacement arrow plot (right).

Fig.5. Convergence of the peeling mode eigenvalues ω^2/ω_A^2 for the doublet equilibrium. Kinetic energy normalization.

Fig.6. External pressure driven kink mode structure for the doublet equilibrium. Normal displacement level lines (left) and displacement arrow plot (right).

Fig.7. Convergence of the external kink mode eigenvalues ω^2/ω_A^2 for the doublet equilibrium. Kinetic energy normalization.

Fig.8. Axisymmetric $n = 0$ resistive wall mode structure for the doublet equilibrium. Normal displacement level lines (left) and displacement arrow plot (right). The TCV vacuum chamber is shown.
a) most unstable mode b) second unstable mode

Fig.9. Convergence of the axisymmetric $n = 0$ resistive modes growth rates $\gamma[s^{-1}]$ for the doublet equilibrium.
a) most unstable mode b) second unstable mode

Fig.10. Axisymmetric $n = 0$ resistive wall mode structure for the divertor equilibrium. Normal displacement level lines (left) and displacement arrow plot (right).

Fig.11. Convergence of the axisymmetric $n = 0$ resistive mode growth rates $\gamma[s^{-1}]$ for the divertor equilibrium.

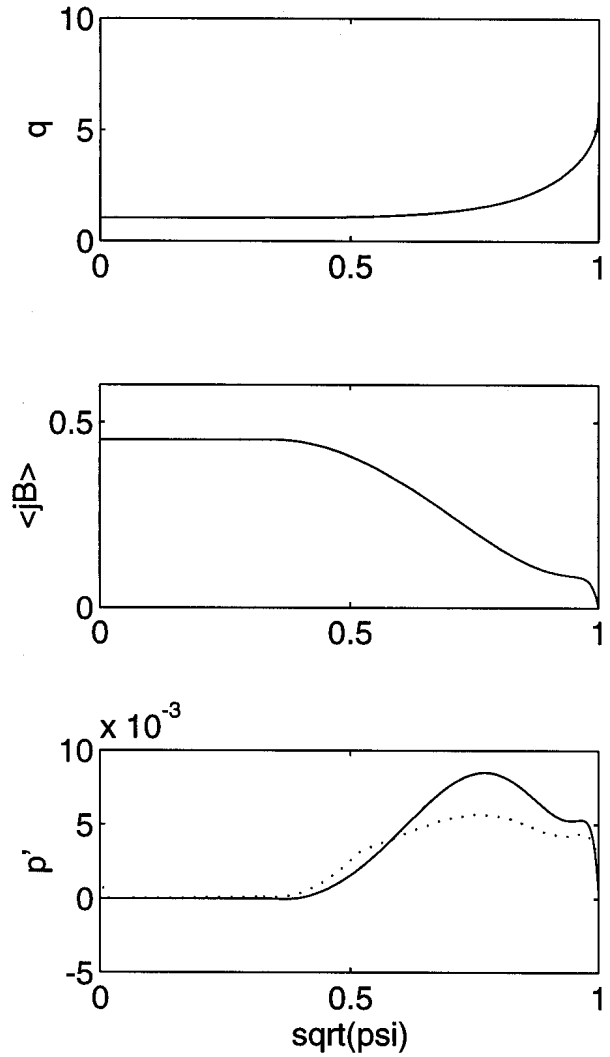

Fig.1

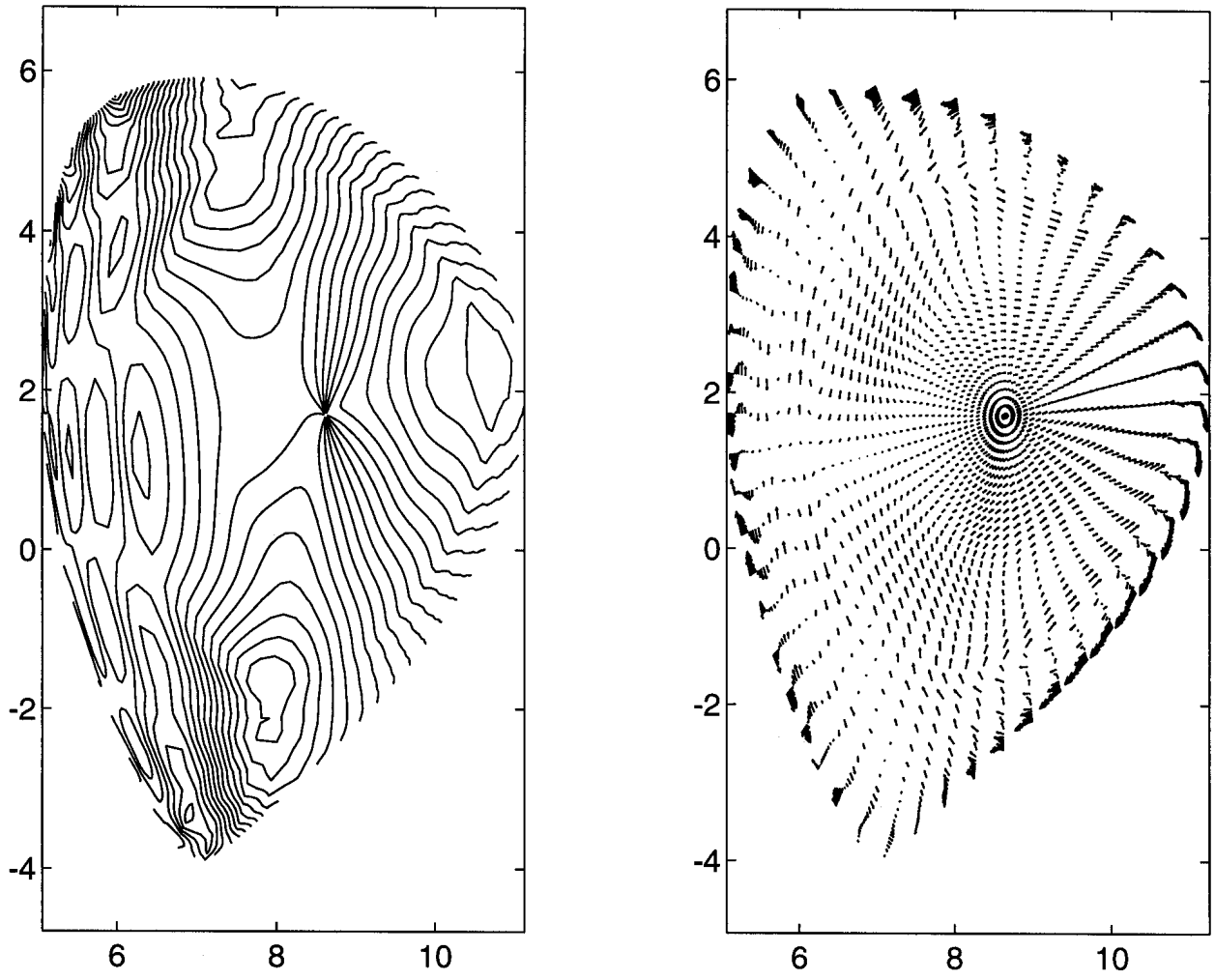

Fig.2

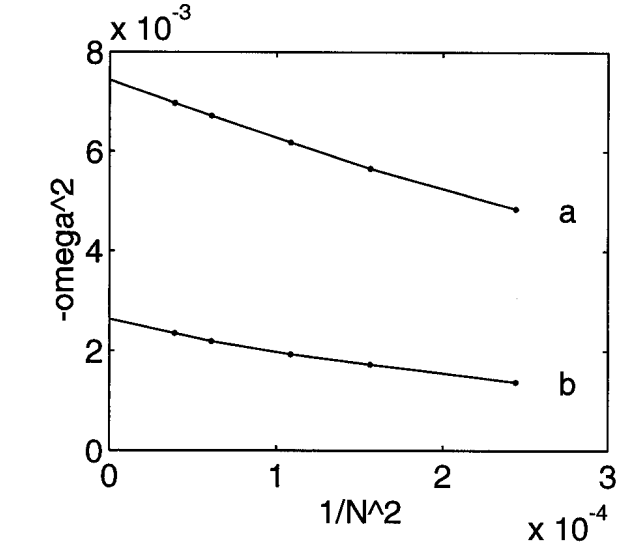
x 10^-3
8
6
4
2
0
-omega^2
a
b
0
1
2
3
1/N^2
x 10^-4

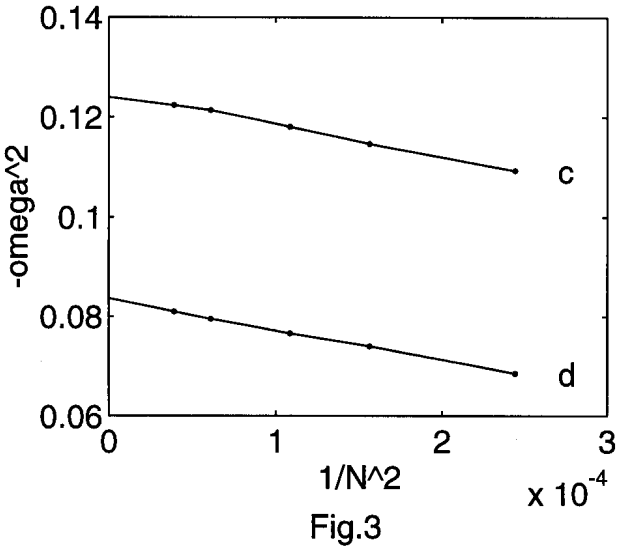
0.14
0.12
0.1
0.08
0.06
-omega^2
c
d
0
1
2
3
1/N^2
x 10^-4

Fig.3

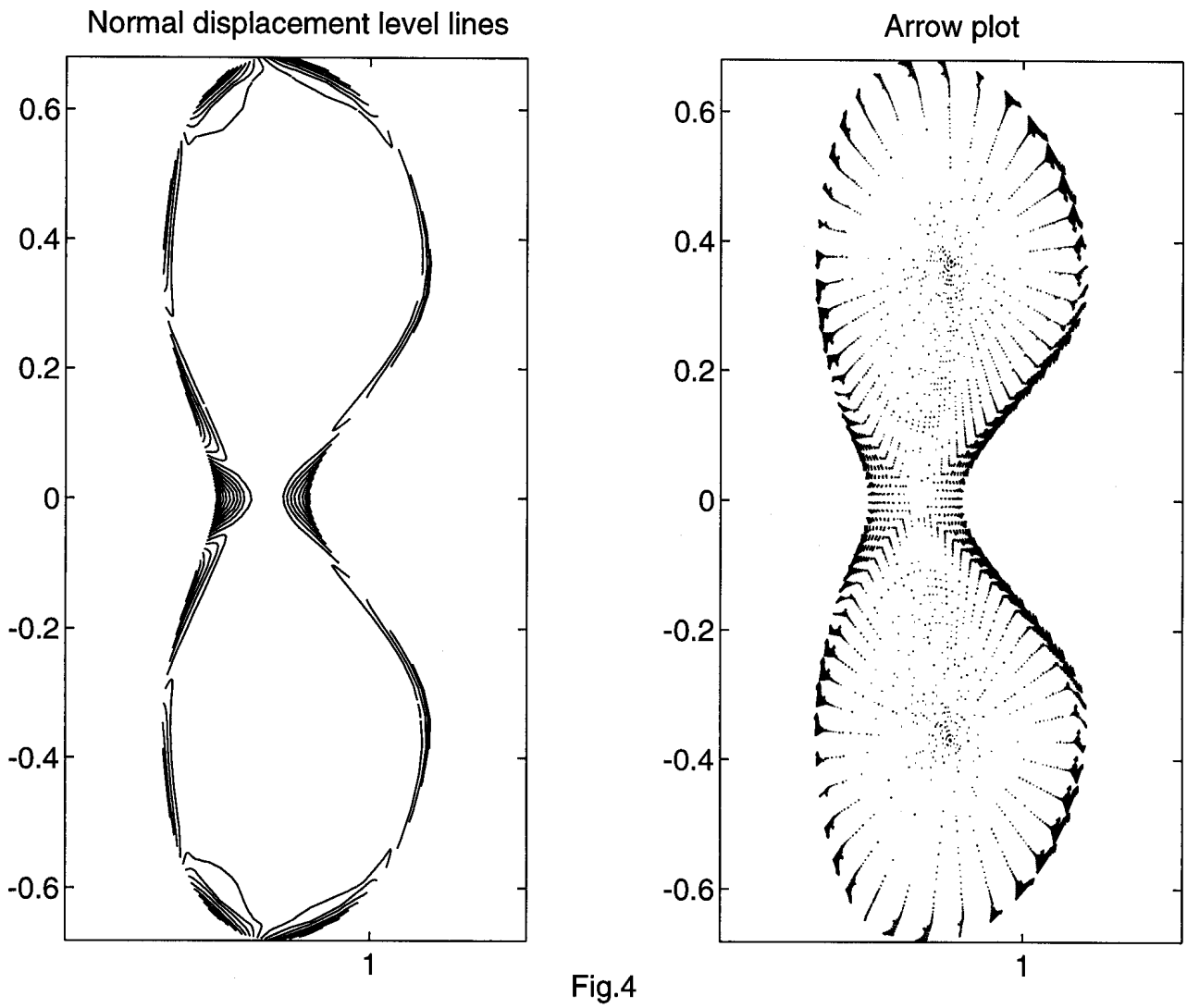
Normal displacement level lines
Arrow plot
0.6
0.4
0.2
0
-0.2
-0.4
-0.6
1
0.6
0.4
0.2
0
-0.2
-0.4
-0.6
1

Fig.4

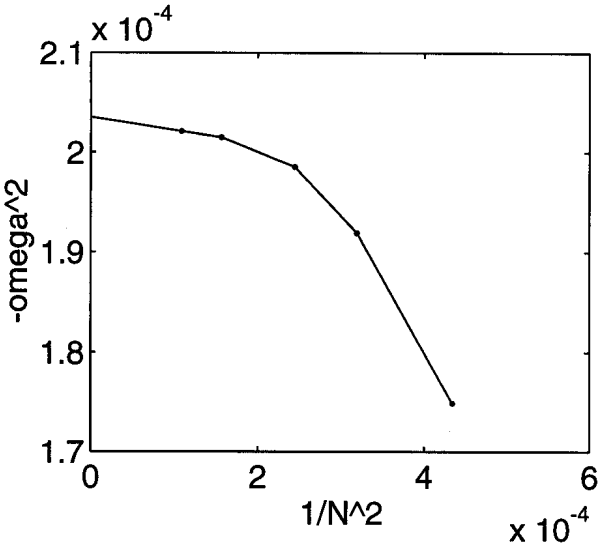

Fig.5

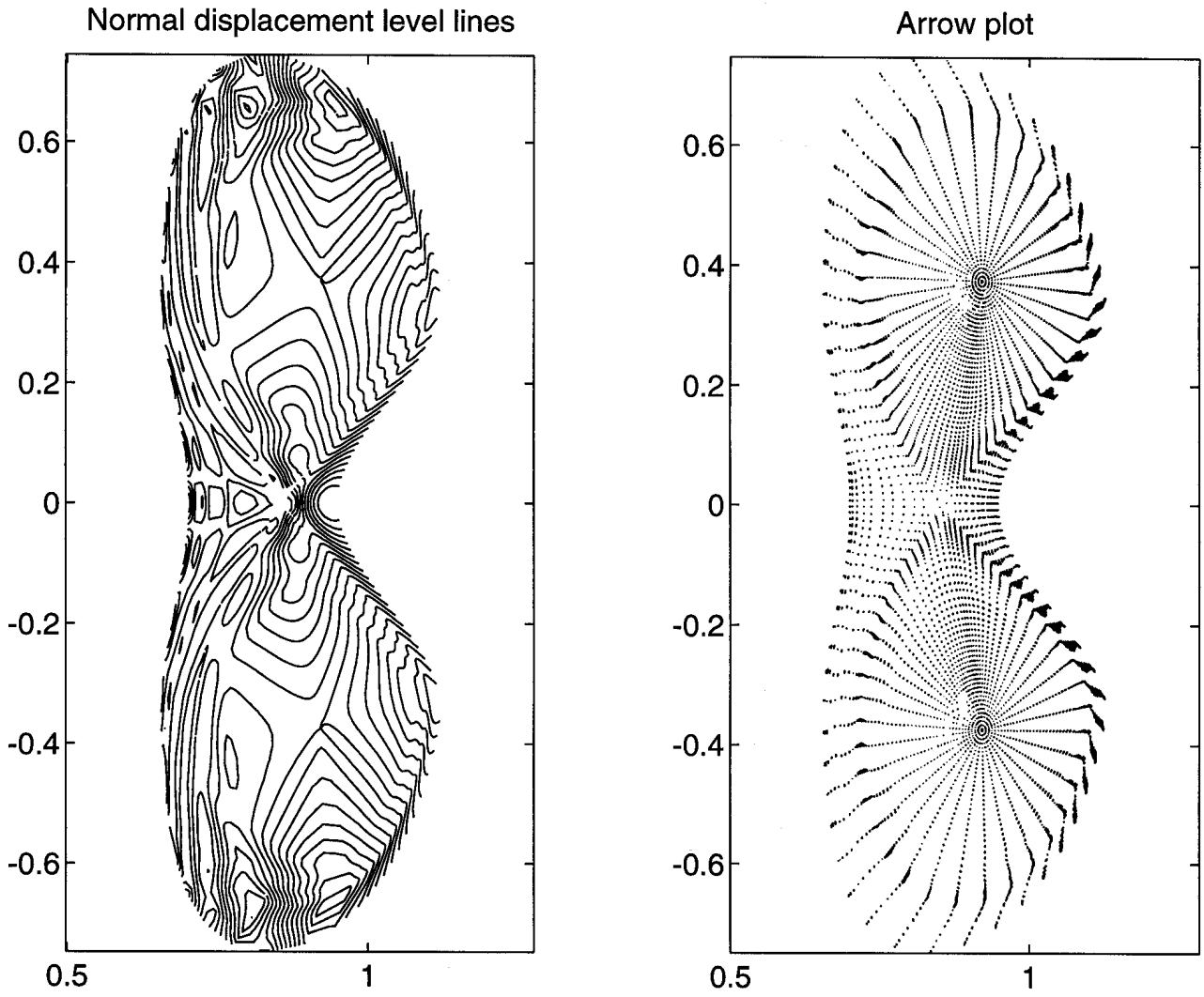
Normal displacement level lines
Arrow plot
0.6
0.4
0.2
0
-0.2
-0.4
-0.6
0.5
1

Fig.6

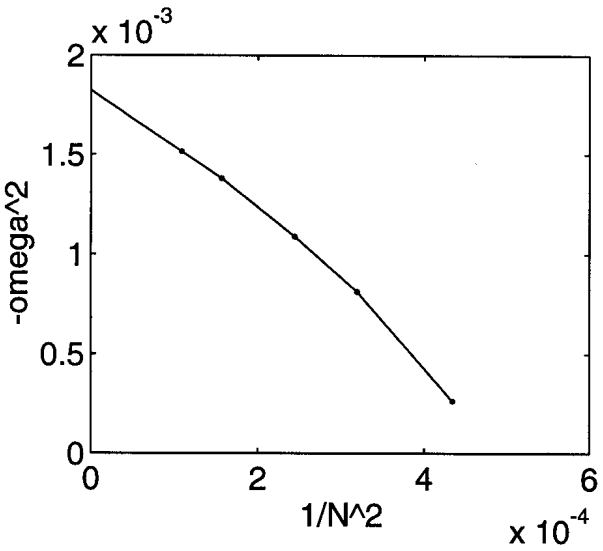

Fig.7

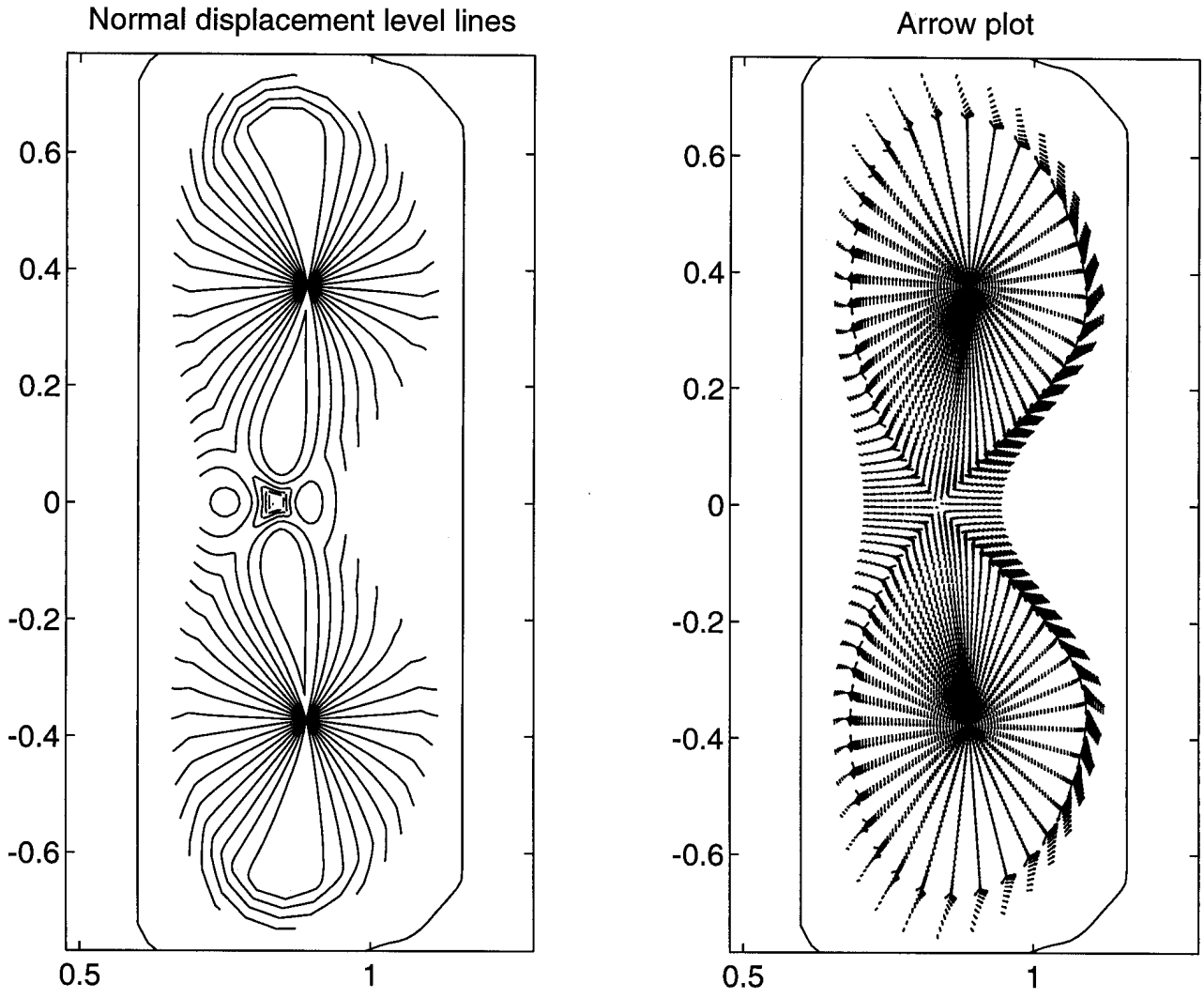
Normal displacement level lines
Arrow plot
0.6
0.4
0.2
0
-0.2
-0.4
-0.6
0.5
1

Fig.8a

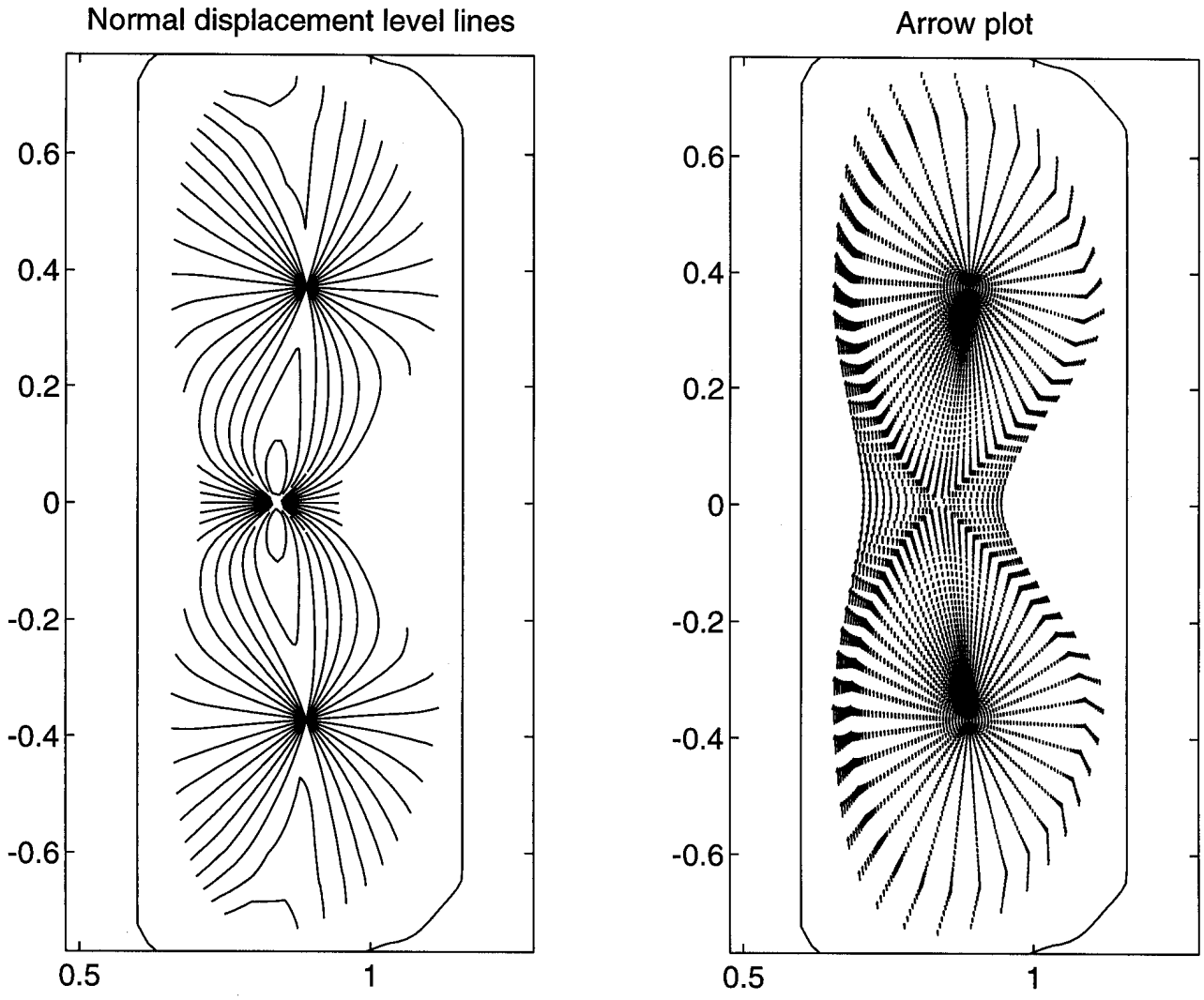
Normal displacement level lines
Arrow plot
0.6
0.4
0.2
0
-0.2
-0.4
-0.6
0.5
1

Fig.8b

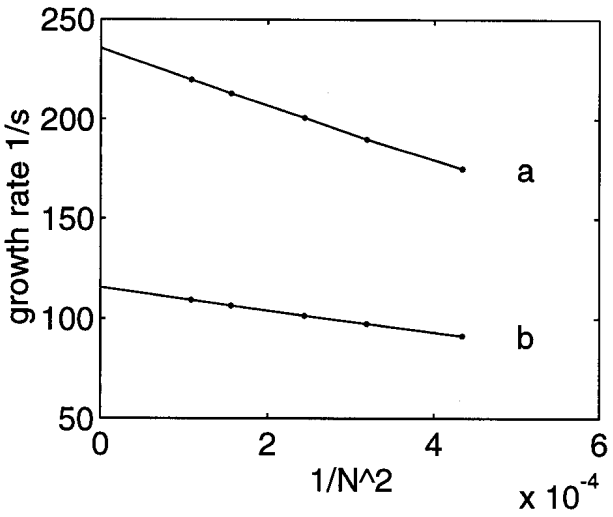

Fig.9

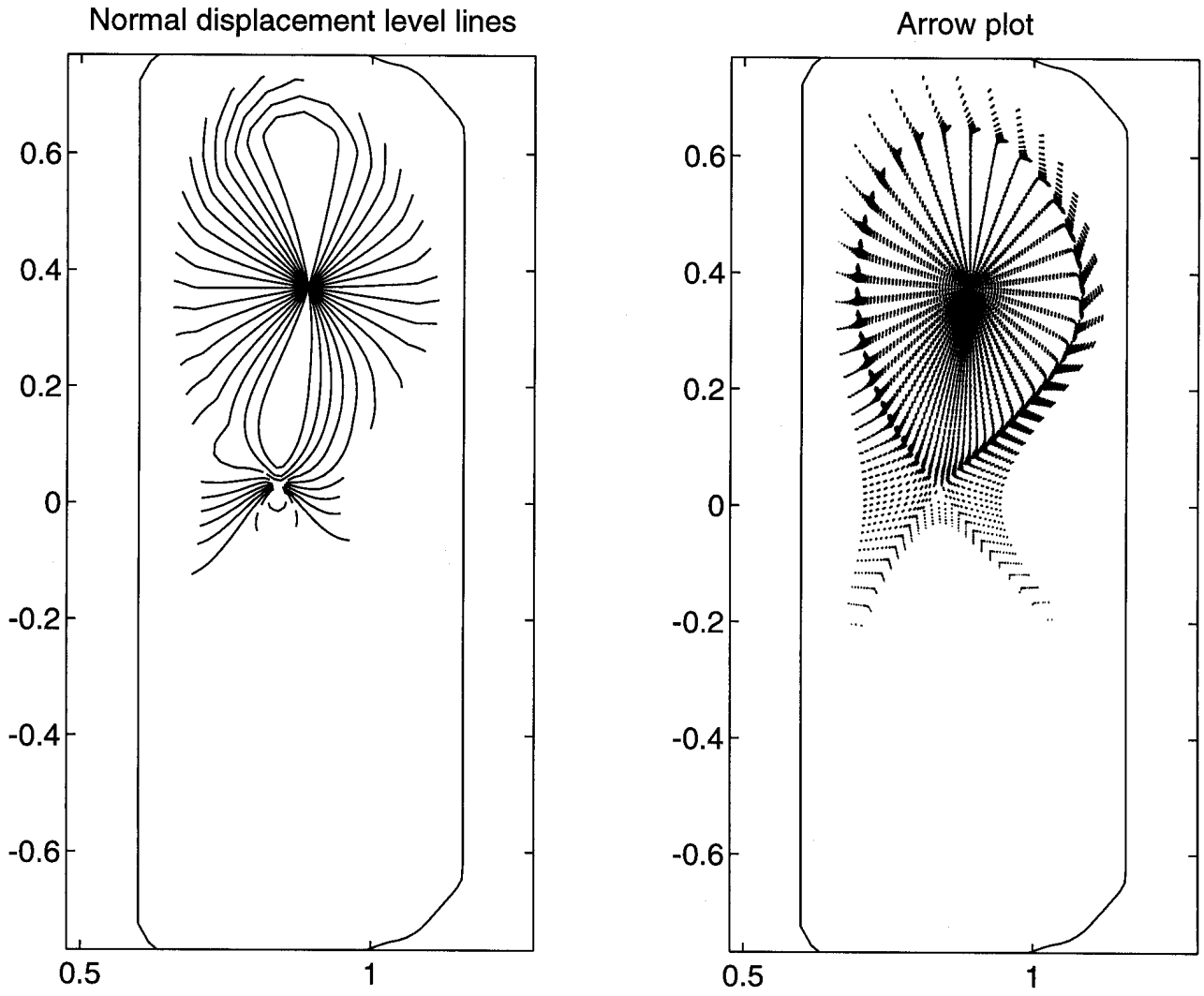
Normal displacement level lines
Arrow plot
0.6
0.4
0.2
0
-0.2
-0.4
-0.6
0.5
1

Fig.10

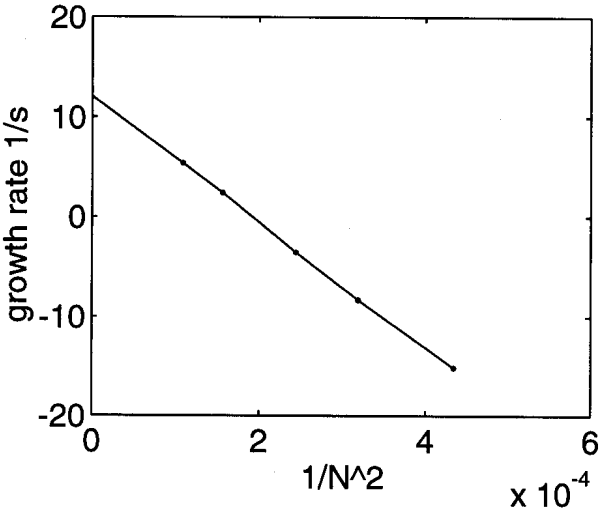

Fig.11